

REV ANALYSIS FOR CARBONATE ROCKS USING PNM FROM MICRO-CT IMAGES AND NMR T₂ DISTRIBUTION

Marianna Dantas

marianna.silva@coc.ufrj.br

Elizabeth M. Pontedeiro

bettymay@petroleo.ufrj.br

Maira Lima

mairalima@coc.ufrj.br

William Godoy

wmgodoy@petroleo.ufrj.br

Paulo Couto

pcouto@petroleo.ufrj.br

LRAP/COPPE/UFRJ

Rua Moniz Aragão 360, Bloco 4, Cidade Universitária, 21941-594, Rio de Janeiro, Brazil

Patrick Machado

patrick_machado@id.uff.br

UFFlar/UFF

Outeiro de São João Batista, s/nº, Centro, 24020-141, Niterói, Brazil

Abstract. Reservoir studies have reached a great advance in the last years with the introduction of microtomography (micro-CT) images of rocks. This technology is a non-destructive method that allows the investigation of internal structure of rock in pore scale, and to build representative 3D models of the rock. With the purpose to retrieve representative petrophysical properties from these digital models, the objective of this work is to apply a Representative Elementary Volume (REV) analysis for the heterogeneous carbonates, considering threshold values, image resolution and NMR pore-size distributions, to estimate porosity and permeability REV's. In this study, carbonate rock samples, Coquina and Edwards Brown, were submitted to three main laboratory measurements: routine core analysis, NMR experiments, and microtomography scans. The micro-CT images were processed using a commercial image processing software. The threshold selection analyzed by applying three methods, but the NMR pore-size distribution oriented threshold was used to proceed with the entire workflow. Skeletons were extracted from pore space binarized in the micro-CT image and exported to PoreFlow for the generation of Pore Network Models (PNM) and permeability estimation. The permeability of the PNMs were estimated considering Hagen-Poiseuille Law to simulate single-phase flow and Darcy's Law. This methodology was applied to three samples of different sizes, their volume was further divided into smaller sub volumes and their relation with REV were analyzed. The rock samples studied could be considered, with a high confidence, as REV for porosity, but only the larger samples could be considered as REV for permeability.

Keywords: REV, Micro-CT, Pore-Network-Model, NMR T₂

1 Introduction

Carbonates reservoirs hold more than 60% of the oil and 40% of the gas volumes present in the world (Schlumberger [1]). This type of reservoir is well known by its heterogeneous properties and the challenges addressed to its characterization. The heterogeneity is an intrinsic rock characteristic resultant of the sedimentary processes the rock is originated from and it is a scale-dependent property, that can vary in both microscopic and macro scale, as in vertical or horizontal directions (anisotropy) in a reservoir (Hurley et al. [2]). When characterizing reservoirs, only a small fraction of the its total volume can be in fact evaluated by core samples or logging tools, therefore many studies work on developing methods to populate, or upscale these properties with higher accuracy.

REV, representative elementary volume, is a methodology developed to help to overcome the challenges addressed by heterogeneity and upscaling. According to Vik [3], Corbett [4][5] and Bear [6], REV is defined as the minimum volume of certain property that is large enough to capture a representative amount of heterogeneity, or the minimum volume that is insensitive to small changes in volume or sample location. Note that REV may vary for different properties of the same rock sample, usually porosity's REV is found in a smaller volume than permeability's REV, due to the latter macroscopic variability. The objective of this study is to apply a REV analysis for porosity and permeability of carbonate rock samples, considering threshold values, image resolution and NMR pore-size distributions.

1.1 Digital Rock Analysis

Petrophysical studies have reached a great advance in the last years with the introduction of microtomography (micro-CT) images of rocks. This technology is a non-destructive method that allows the investigation of internal structure of rock in pore scale, it uses the capability of radiation to penetrate materials in varying degrees, which depends mainly on their density, to produce images of the material (Bultreys [7]). Image processing techniques allow to build representative 3D models of the rock that can be investigated to estimate petrophysical properties.

One of the methods applied to simulate multi-phase flow in porous media at pore-scale and thus, to estimate petrophysical properties, are Pore Network Models (PNM) (Bultreys [7]). According to Blunt [8], PNMs are a simplified representation of the complexity of the pore space with idealized geometries such as spheres. These models have been proved success in representing the multiphase behavior in a pore scale at a low computational cost (Blunt [8]).

The pore space is a continuous, and thus it can be discretized by elements. Pores can be identified as the larger open spaces, while pore-throats are characterized as constrictions to the flow. According to Bultreys [7], there are two classes of methods to discretize the pore space: topology-central methods and morphology central methods. The first, applies a medial axis algorithm, which is an approach to represent the pore space by a centralized skeleton that can be used to detect individual pores and throats (Figure 1). The latter, morphology-central methods, generally applies search vectors to first identify constrictions, and then characterize the pore. One of the morphology-methods applies a maximal-ball algorithm (Figure 2). This method runs a search vector and tries to fit the largest inscribed sphere centered on each image voxels defined as pore-space. Afterwards, the spheres are classified into families, where the largest balls are classified as family ancestors (pores) and the smallest, or narrow passages, to belonging to that family (throats).

The PNMs generated can capture important features that impact the fluid flow in porous media such as constrictions, pore-size distributions and coordination number (number of pore connections). To get estimates of permeability out of those simplified geometry networks, one can simulate single-phase fluid flow in the network and apply Darcy's equation to the volume.

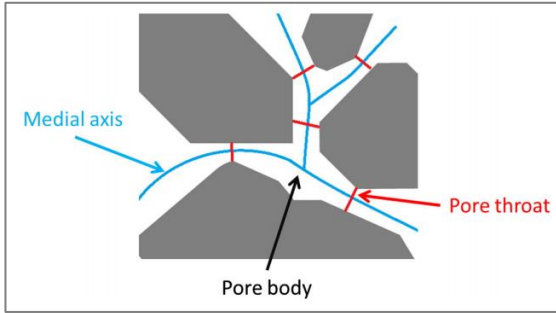


Figure 1: Representation of a section of pore space, its medial axis and throats identified by applying a medial axis algorithm. Reproduced from Bultreys [7].

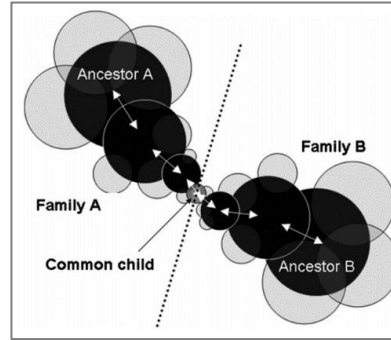


Figure 2: Maximal balls algorithm classification of pore bodies in families A and B, which are represented by an ancestor (pore) and throats (connecting spheres). Reproduced from Bultreys [7].

PoreFlow (Raof et al. [9][10], Vries et. al.[11] is pore-scale simulator with capabilities that includes pore network generation, drainage simulation, calculation of pressure and velocity distribution and modeling of flow and (reactive) transport in pore-scale. We apply this software package for PNM modeling and fluid flow simulation for permeability determination. In this application, its pore network model considers a porous medium as a system of pore elements composed of pore-bodies, which are denoted by spheres, and pore-throats, denoted as cylinders (Figure 3).

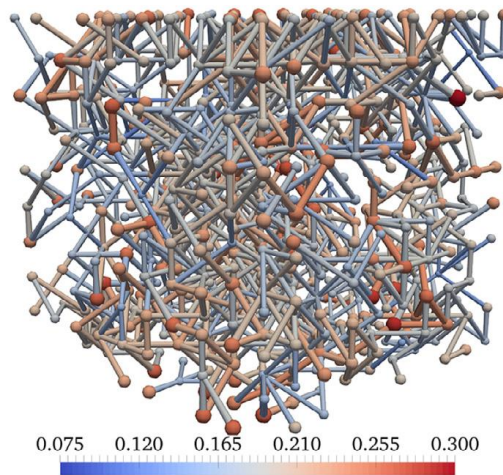


Figure 3: Pore network model represented by simplified geometries, such as spheres and cylinders. Reproduced from Vries [11].

The flow simulation in PoreFlow is performed by establishing a pressure difference across the network in one direction to meet a boundary condition of constant flow rate. According to Raof et Al. [10] and Vries et al. [11], PoreFlow assumes that, assuming a laminar flow for, the flow in a given pore throat can be defined by the Hagen-Poiseuille equation:

$$q_{ij} = g_{ij} (p_j - p_i) \quad (1)$$

where $q_{ij,tot}$ is the volumetric flow rate through a given pore throat ij , between the pore-bodies i and j , and p_i and p_j their respective pressures, while g_{ij} is the conductance of the throat, that can be represented as the Equation 2, if its geometry is considered as a cylinder:

$$g_{ij} = \frac{\pi R_{ij}^4}{8\mu l_j} \quad (2)$$

where μ represents the fluid viscosity, l represents the cylinder length, and R_{ij} the cylinder radius. Assuming the condition of incompressible flow, where the sum of fluid into and out of a pore-body must be zero and given the z_i as the pore coordination number of pore i , the continuity equation may be considered as:

$$\sum_{j=1}^{z_i} q_{ij} = 0; \quad j = 1, 2, 3, \dots, z_i \quad (3)$$

Therefore, according to Vries et. Al. [11] the average fluid velocity can be defined as:

$$v = \frac{Q_{tot} L}{V_f} \quad (4)$$

where Q_{tot} is the total discharge of the pore network, L is the total length of the pore network, and V_f the total volume of fluid in the pore network. Therefore, the permeability of the pore network can be expressed as Darcy's equation below:

$$k = \frac{\mu Q_{tot} L}{A \Delta P} \quad (5)$$

where A is the cross-section area of the pore network and ΔP is the differential pressure between the pore network inlet and outlet.

1.2 NMR T₂ Distributions

NMR physical principles rely on the Hydrogen Nuclei Relaxometry, that is, the response of a nuclei to a magnetic field. According to Kenyon [12], hydrogen nuclei have a magnetic moment and spin, that, when exposed to an induced external magnetic field (B_0) get its spins gradually aligned towards the field B_0 . To study the relaxation behavior of the spin one applies radio-frequency pulses to generate a secondary magnetic field (B_1) which cause a perturbation in the thermal equilibrium between the spin orientation and the main magnetic field (B_0), the time in which the spin returns to its thermal equilibrium after the radio-frequency pulses are applied is the so called relaxation time.

Hydrogen nuclei are mainly present in the fluid's molecules confined inside the rock pores, and based on this fact, rock and fluids properties can be driven from such signal emitted by the magnetic field during the relaxation time. Kenyon [12] attested that those relaxation times can be measured from both longitudinal and transverse proton magnetization, which are two simultaneous and independent mechanisms. The curve entitled T_1 is the relaxation time correspondent to the longitudinal, that is, in the same direction as the external field applied to it. On the other hand, T_2 resembles the transversal relaxation time to the related field. T_2 relaxation curves were used in this study.

According to Coates [13], when a wetting fluid fills a porous medium like a rock, T_2 decreases and the relaxation mechanisms are different from the measurements in only a solid or a fluid. In this case, the mechanism that rule T_2 are: bulk fluid, surface relaxation and diffusion. The equation that define these three processes is:

$$\frac{1}{T_2} = \frac{1}{T_{2bulk}} + \frac{1}{T_{2surface}} + \frac{1}{T_{2diffusion}} \quad (6)$$

The bulk relaxation (T_{2bulk}) is the individual relaxation of the fluid, and it is controlled by its physical properties such as viscosity and molecular composition. The diffusion relaxation ($T_{2diffusion}$) occurs when fluids such as gas, light oil or water show a gradient magnetic field, as result the final T_2 is

shortened. And finally, the surface relaxation ($T_{2surface}$), which is the response to the pore wall contact with the fluid saturating it, where the response time increases according to the pore size (Figure 4). This effect provides sensitivity of NMR to pore size and brings the possibility to correlate rock parameters to it. Surface relaxation (Equation 7) is controlled by surface relaxivity, which varies with the rock mineralogy.

$$\frac{1}{T_{2surface}} = \rho_2 \left(\frac{S}{V} \right) \quad (7)$$

In equation 7, S/V is a measure of pore size, it is the ratio of pore surface to fluid volume. Thus, the lowest the surface by the volume ratio, the longest T_2 and larger the pore is. For lab-based rock NMR experiments, usually saturated with brine, the final T_2 is dominated by $T_{2surface}$, thus, the effect of the other components may be neglected (Kenyon et. al. [12], Coates et. al[13], Souza et. al [14],).

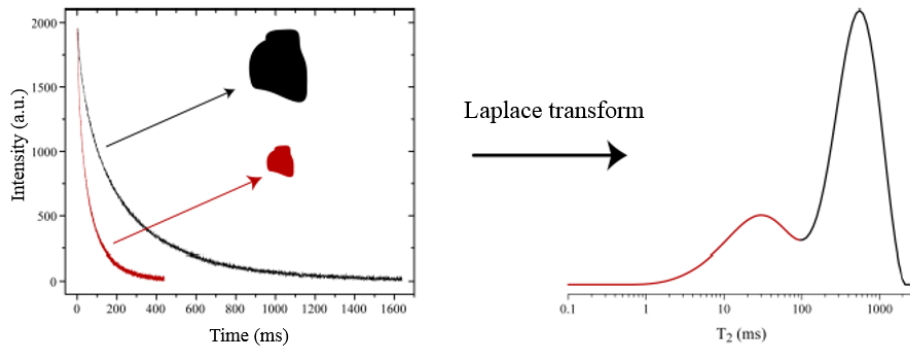


Figure 4: Inversion process of T_2 echo train to T_2 distribution vs porosity increment. Reproduced from Souza [14].

The interpretation of the T_2 distribution (Figure 4) in terms of pore-size can be performed by the equation 7. Assuming the pore as spheres and knowing the rock surface relaxivity, T_2 can be converted to length, and analyzed as pore size (Souza et. al. [15]). According to Hoerlle et al. [16][17] the pore-size distribution encountered in NMR T_2 can be correlated to the pore-size observed in the micro-CT images. Assuming the minimum diameter that a pore is identified in an image is represented by one single pixel, the micro-CT image is able to estimate pores with diameter above this resolution. Therefore, the micro-CT is able to characterize up to the total porosity from the NMR pore-size distribution above that diameter.

2 Material and Methods

In this study, carbonate rock samples were submitted to three main laboratory measurements: routine core analysis (RCA), NMR T_2 experiments, and microtomography scans. The samples studied were the coquina A_34 and three samples of the limestone Edwards Brown:

Table 1: Samples data acquisition.

Sample	RCA	NMR T_2	Micro-CT	Diameter/L (mm)	Thickness (mm)
1_34A	x	x	x	36.0	35.3
EB_1			x	25.0	4.0
EB_2	x		x	37.5	13.0
EB_3	x	x		37.2	200.0

The data acquired for the coquina 1_34A was kindly released by Hoerlle et al. [16] and Godoy et al. [18].

The coquina analyzed in this study is originated from the Morro do Chaves Formation, located in Sergipe-Alagoas Basin, Northeast Brazil. According to Hoerlle et al. [16] it is a bioclastic rock, formed mainly by lacustrine bivalves that suffered several processes of diagenesis. The Edwards Brown samples were acquired at Kocurek Industries and they are limestones originated from a layer in the Austin Chalk formation, located in Texas, USA.



Figure 5: Samples EB_1, EB_2, 1_34A and EB_3

2.1 Methods

Data Acquisition

Routine core analysis was performed to measure the rock properties for porosity and permeability. The porosity and permeability were acquired using gas instruments at the Enhanced Oil Recovery Laboratory (LRAP/COPPE/UFRJ).

The micro-CT images were kindly acquired by the team at Nuclear Instrumentation Laboratory (LIN/COPPE/UFRJ). The equipment used to the acquisition was SkyScan 1173, a high energy micro-CT scanner for dense objects (Bruker). The x-Ray source was operating with a current of approximately 133 uA and 60 kV and it was used a flat aluminium filter of 1 mm. In this acquisition process, the x-rays source is stationary and the samples placed in a rotating core holder, which rotated 360° with steps of 0.5° during the acquisition. The images reconstruction was also performed by LIN using the software package NRecon version 1.6.9.4. The resolution for each sample is presented in the table below:

Table 2: Samples image resolution.

Sample	Resolution (um)
1_34A	18.16
EB_1	17.81
EB_2	12.46

NMR T₂ curves for the sample EB_1 were acquired at the *Laboratório para Aplicações de RMN e Petrofísica* (UFFlar/UFF). The pore-size distribution was obtained by the conversion of the NMR T₂ curve, considering pores as spheres and their surface relaxivity, a parameter usually inverted from the DT₂ experiment. After Luna et. al. [19] the average surface relaxivity was adopted as 35.7 um/s. The EB surface relaxivity value of 23.6 was adopted as an averaged value based on similar carbonate rocks presented by Souza et. al. [15].

Images and PNM Processing

The micro-CT images were processed using the commercial software Avizo 9.5. The raw image was first filtered using the filter Non-local Means Avizo [20], then cropped and segmented. The threshold selection was first analyzed manually and by applying Otsu’s algorithm (Avizo [20]). After segmentation, the images were analyzed by their estimated porosity, which is defined as the number of pixels correspondent to the pore space divided by the total number of pixels of the rock. Finally, the result was compared, and threshold was adjusted to the correspondent porosity from NMR pore-size distribution curve:

$$\Phi = \frac{N_p}{N_t}, \quad \text{where } N_t = N_p + N_m \tag{5}$$

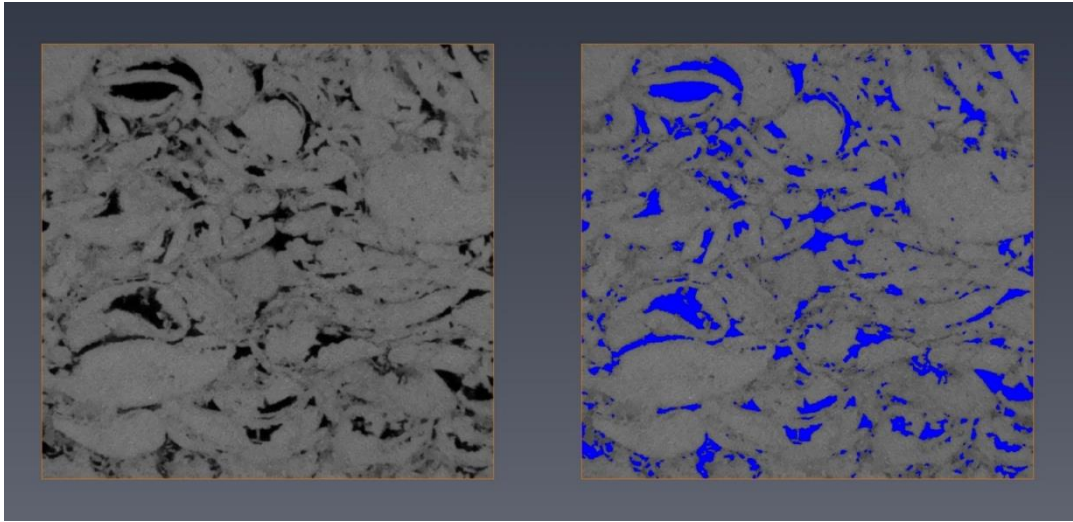


Figure 6: Filtered micro-CT image and segmented micro-CT image.

PNM Skeletons were extracted from pore space binarized in the micro-CT images using the methodology of Maximal-balls. A Mathematica code was used to transform these “spheres” pore and throats to “spheres” and “cylinders” representing pore and throat. The main change occurred to the throat’s geometry. For this transformation, the Euclidean distance between the pore centers was calculated and defined as the length of the cylinders, while an arithmetic average of the spheres radius was calculated and assumed as the cylinder radius. Later, the processed skeleton was exported to PoreFlow, a simulation software, for the generation of Pore Network Models (PNM), fluid flow and permeability estimation. The permeability of the PNMs were estimated considering Hagen-Poiseuille Law to simulate single-phase flow and Darcy’s Law according to equations 1-5.

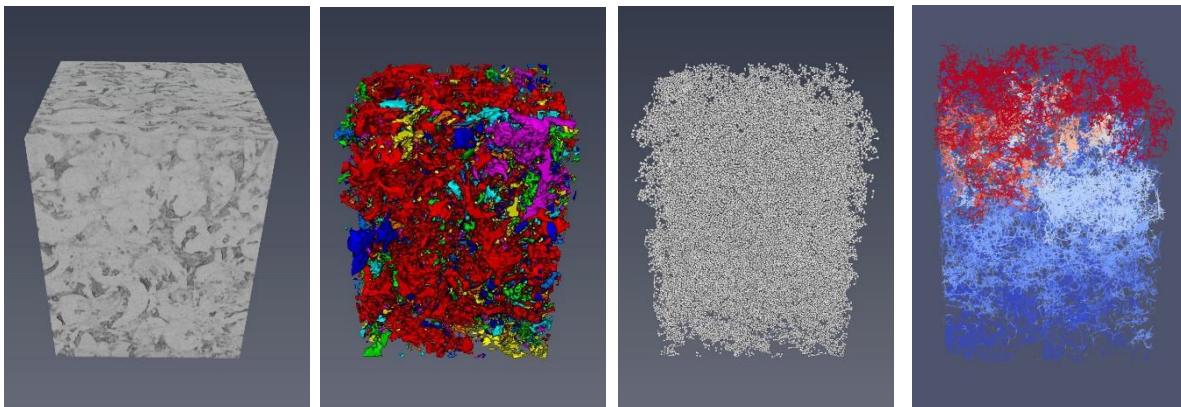


Figure 7: Sample 1_34A: Rendered volume, connected pore space, PNM skeleton, and PNM flow simulation pressure field.

The methodology to estimate petrophysical properties from the micro-CT images was applied to the three samples of different sizes, the coquina 1_34A, the plug EB_2 and its twin slab EB_1, which was imaged with higher resolution. Their volume was divided into smaller sub volumes for REV analysis, according to the Figure 8. Sample 1_34A was divided up to 8 subvolumes, while EB_1 and EB_2 where divided up to 4 subvolumes.

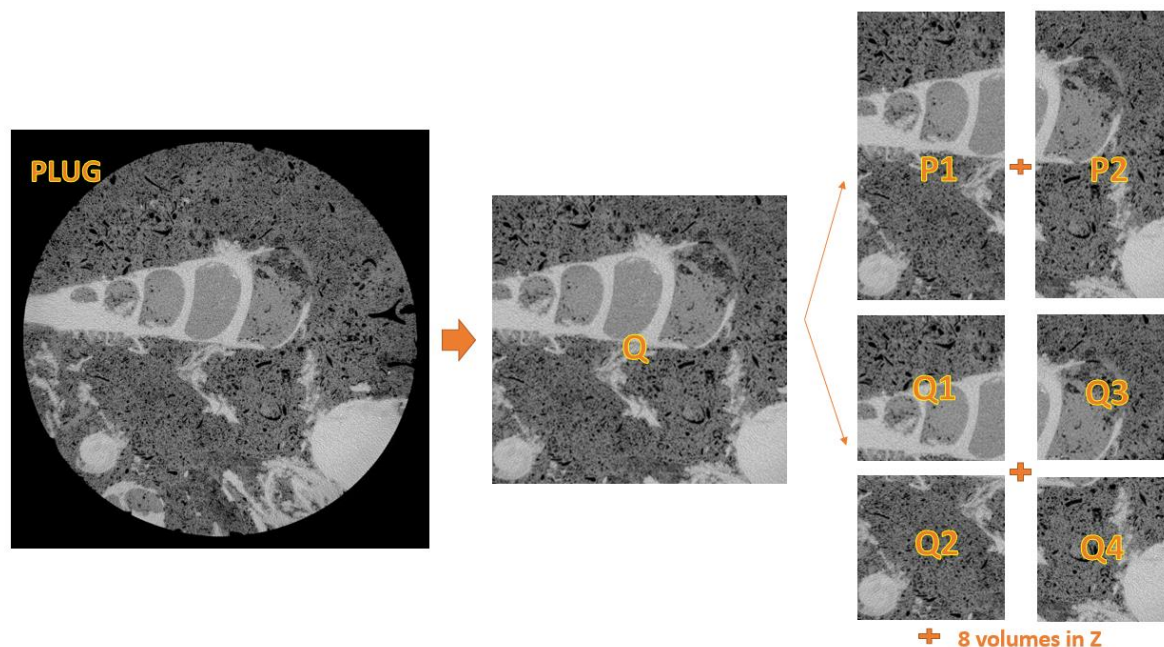


Figure 8: Volume subsampling for REV study.

The following volumes division were adopted for each sample:

Table 3: Subsamples Division volumes in mm³

Sample	Plug	Volume in mm ³			
		Inscribed square (Q)	1 st division (P1/P2)	2 nd division (Q1/Q2/Q3/Q4)	3 rd division (8 volumes in Z)
1_34A	21845.97	13775.0	6887.5	3443.8	1721.88
EB_1	-	690.83	345.42	172.71	-
EB_2	9710.68	5999.95	2999.97	1499.99	-

3 Results and Discussion

The results from routine core analysis are show in Table 4. The measured results were further used in this paper for comparison with the values por porosity and permeability estimated from the images. According to Kurotoria [21] Edwards Brown samples present microporosity, which can be observed comparing the results from the coquina 1_34A and EB for micro-CT images, porosity-permeability ratio and NMR pore-size distribution.

Visually comparing both samples in the micro-CT images (Figure 9), it is possible to identify that, in general, the pores in the EB sample are smaller and in higher quantity, while on the coquina 1_34A sample, pores are likely to be larger and better defined by the images of about the same resolution. The presence of the microporosity may cause to the low permeability to porosity ratio of the EB samples compared to the coquina sample, while EB holds an average of 31-33 % of porosity and only 300-400 mD of permeability, the coquina sample presents 639 mD of permeability for only 16.4% of porosity. These values show that the pore-network of the coquina sample is better connected than the EB samples. Looking at the perspective of the NRM pore-size distribution, if an average image resolution of 18

microns is assumed for both samples, up to 75% of the total NMR porosity can be analyzed for the coquina, that is, 75% of the pore diameters are over 18 microns. If the same is considered for the EB sample, only 42.5% of the pore diameter are over 18 microns.

Table 4: RCA for samples studied.

Sample	Porosity (%)	Permeability (mD)
1_34A	16.3	639.0
EB_2	31.4	314.4
EB_3	33.6	408.0

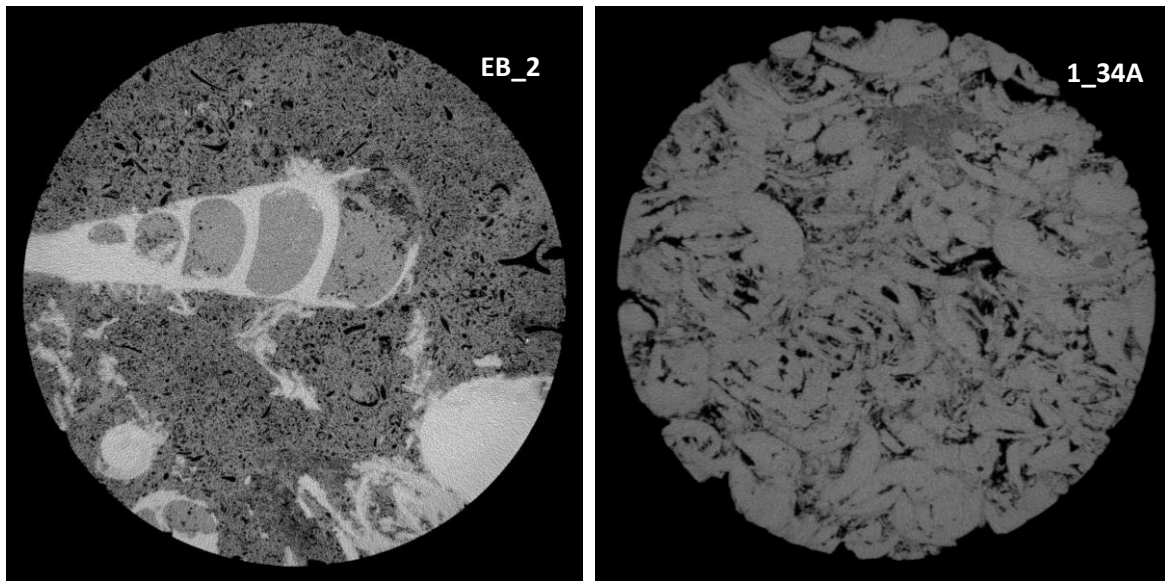


Figure 9: Micro-CT images of samples EB_2 (17.81 μm) and 1_34A (18.16 μm)

NMR T_2 – Pore size distribution

The NMR T_2 curves acquired for the EB samples and the coquina (Hoerlle [17]) were converted from T_2 in ms (Figure 10 and Figure 11) to length in micron by applying equation 7. The surface relaxivity values were assumed as 35.7 and 23.6 for the coquina and Edwards Brown, respectively. The surface to volume ratio was considered as 3 as we assumed pore as perfect spheres. The results are plotted in Figure 12 and Figure 13. Both plots are composed of a blue line (real data) and the red dotted line, that represents the portion of porosity that can be visualized by the images of 18.16 μm (1_34A) and 17.81 μm (EB_2), considering that the minimum pixel size is equivalent to the minimum pore diameter that can be observed by that image. The results of the threshold value estimated according to the NMR pore-size distribution will be discussed in the next section.

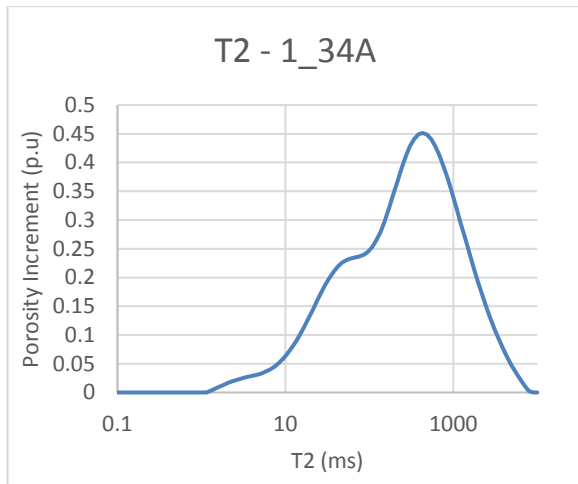


Figure 10: T₂ distribution of sample 1_34A.

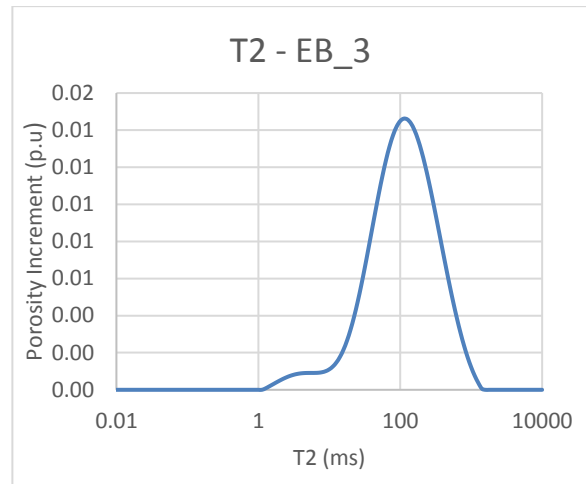


Figure 11: T₂ distribution of sample EB_3.

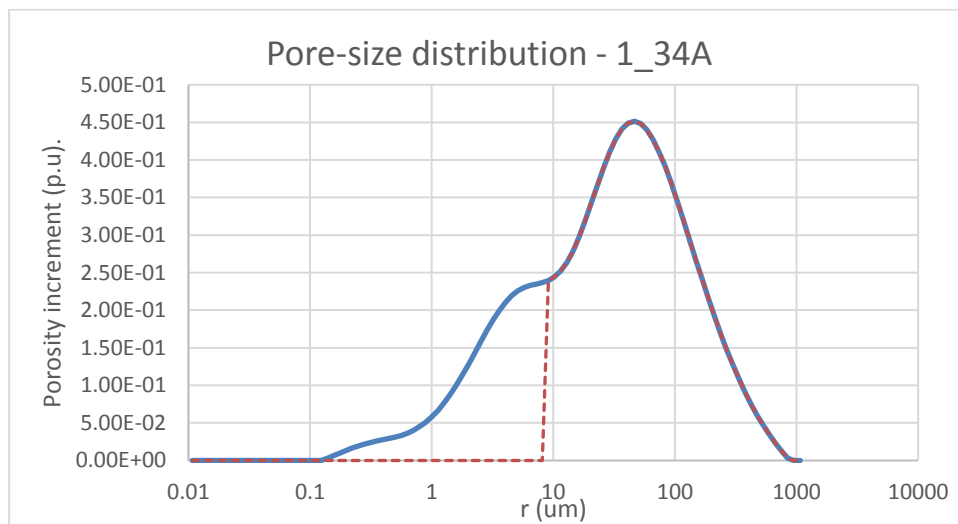


Figure 12: NMR pore-size distribution of sample 1_34A.

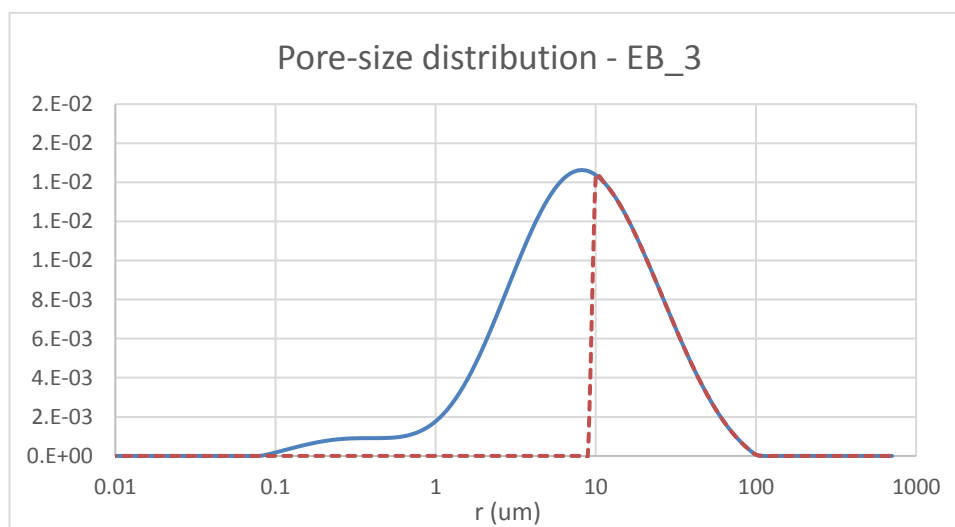


Figure 13: NMR pore-size distribution of sample EB 3.

Threshold values

Three methods for segmentation were applied to the samples' images (Table 5): manual, Otsu's algorithm and NMR threshold. The manual selection is done by visual evaluation, and thus, is submitted to user dependency. This method resulted in the most conservative values for threshold and porosity result represented around 56%, 20% and 56% for EB_2, EB_1 and 1_34A respectively, of the value measured in laboratory. Moreover, in the scenario of the Edwards Brown samples, which were imaged at different resolutions (Figure 14), it is possible to observe the difference of porosity estimated considering the same threshold value. In the case of this sample, the pores under de diameter of 17.81 are responsible for a large amount of the total porosity.

The threshold values estimated by Otsu's algorithm reflect to a more optimistic scenario if compared to the manual selection, and also optimistic if compared to NMR thresholds for the samples EB_2 and 1_34A. The porosity values considering the estimated threshold represent 77% for the coquina, and 82% and only 36% for EB_1 and EB_2 respectively, if compared with the lab measurement for the sample EB_2.

Table 5: Thresholds evaluated for images segmentation.

Sample	Resolution (um)	Threshold (manual)	Threshold (Otsu)	Threshold (NMR)
1_34A	18.16	54	72	64
EB_1	17.81	43	61	70
EB_2	12.46	58	80	65

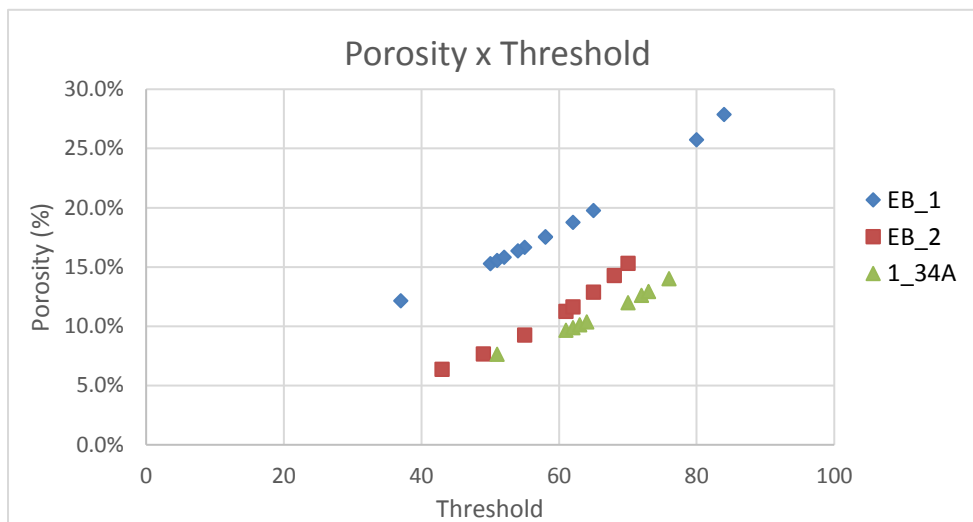


Figure 14: Porosity variation against threshold of segmentation for samples EB_1, EB_2 and 1_34A.

Finally, the threshold value applied to the workflow was determined after the boundaries established by the NMR pore-size distribution. Although the manual selection seems too conservative and the Otsu may be too optimistic, NMR pore-size distribution is able to present a physical measurement to define the segmentation threshold. Table 6 shows in the first column, the total NMR porosity of each sample, and the maximum porosity estimated by the micro-CT image at its resolution. The second column show the threshold value used, and the third column shows the porosity estimated by the micro-CT images. The last column shows the percentual errors calculated between the maximum porosity estimated by the resolution and the final porosity estimated.

Table 6: Comparison of porosities expected at each resolution and result porosity value for threshold.

NMR porosity vs. micro-CT porosity				
	Porosity (NMR) (%)	Threshold	Micro-CT Porosity (%)	Error (%)
1_34A (measured)	13.96	-	-	
1_34A (18.16 um)	10.44	64	10.37	0.67
EB_3 (measured)	33.6	-	-	
EB_1 (12.46 um)	20.08	65	19.78	1.49
EB_3 (17.81 um)	15.7	70	15.3	2.55

REV analysis - Porosity

The porosity was estimated to a total of 1 sample and 15 subsamples for the coquina 1_34A. The plug was first analyzed, second the maximum square inscribed in its radius. Then, in the XY direction it was divided into other two squares, which were then, divided into other two squares. Ultimately, the four last squares were divided by two in the Z direction. The results for the porosity estimated for each subsample and sample are plotted as a function of sample volume in the Figure 15. From the 15 subsamples analyzed only one presented a variation from the sample higher than 10%. Therefore, considering a confidence percentage 94% percent, samples above approximately 3400 mm³ can be considered as REV for porosity for the coquina sample 1_34A.

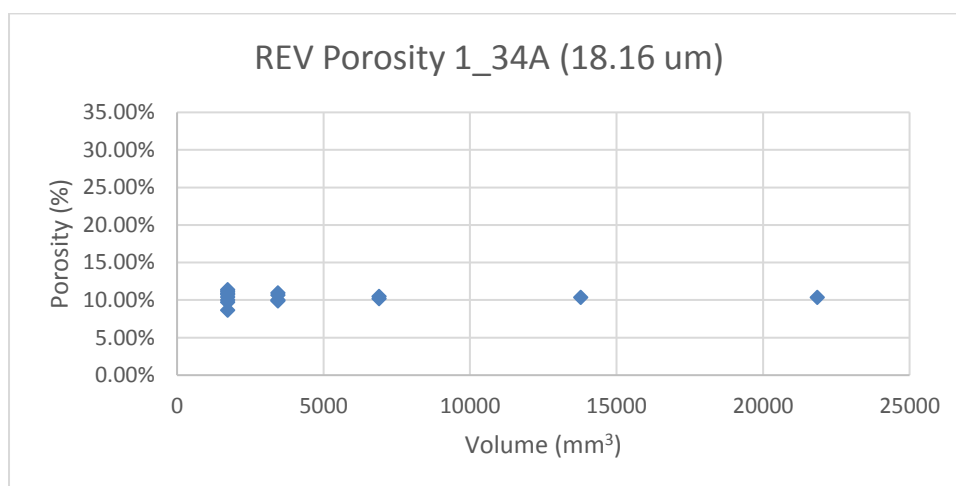


Figure 15: REV analysis for porosity of sample 1_34A.

The porosity was estimated to a total of 1 sample and 6 subsamples for the carbonate EB_1. The total volume of the slab was first analyzed, then, in the XY direction it was divided into other two squares, which were then, divided into other two squares. The results for the porosity estimated for each subsample and sample are plotted as a function of sample volume in the Figure 16. From the 4 subsamples that presented a volume approximately 170 mm³, only one sample showed a variety higher than 10%. Therefore, considering a confidence percentage 99% percent, the subsamples above approximately 350 mm³ can be considered as REV for porosity for the Edwards Browns EB_1.

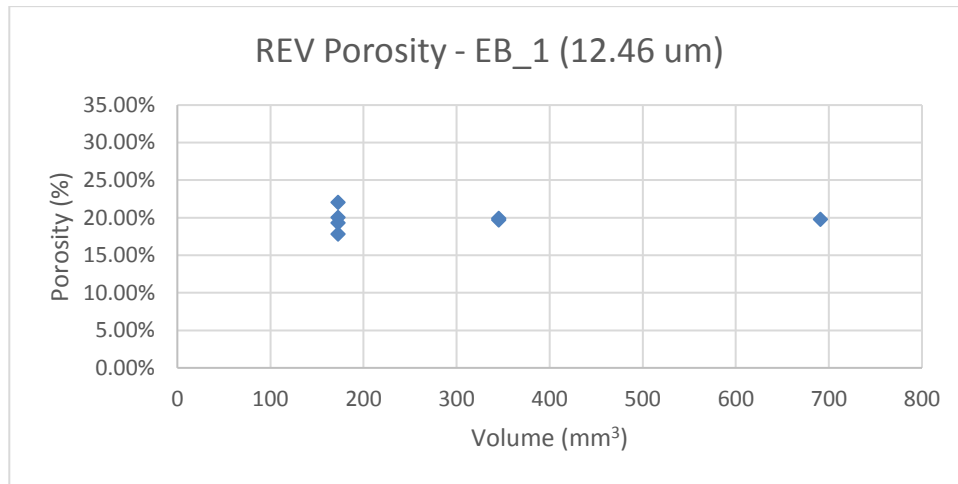


Figure 16: REV analysis for porosity of sample EB_1.

The porosity was estimated to a total of 1 sample and 7 subsamples for the carbonate EB_2. The plug total volume was first analyzed, second the maximum square inscribed in its radius. Then, in the XY direction it was divided into other two squares, which were then, divided into other two squares. The results for the porosity estimated for each subsample and sample are plotted as a function of sample volume in the Figure 17. Due to the high heterogeneity, also represented by the number of shells found in the volume studied, this sample presented a large variety of porosity. Consequently, at the second degree of subsampling a value of 13.8% percentual error could be found. For this reason, we recommend, with a confidence percentage of 91.4%, that volumes above approximately 6000 mm³ to be used for the study of porosity this sample.

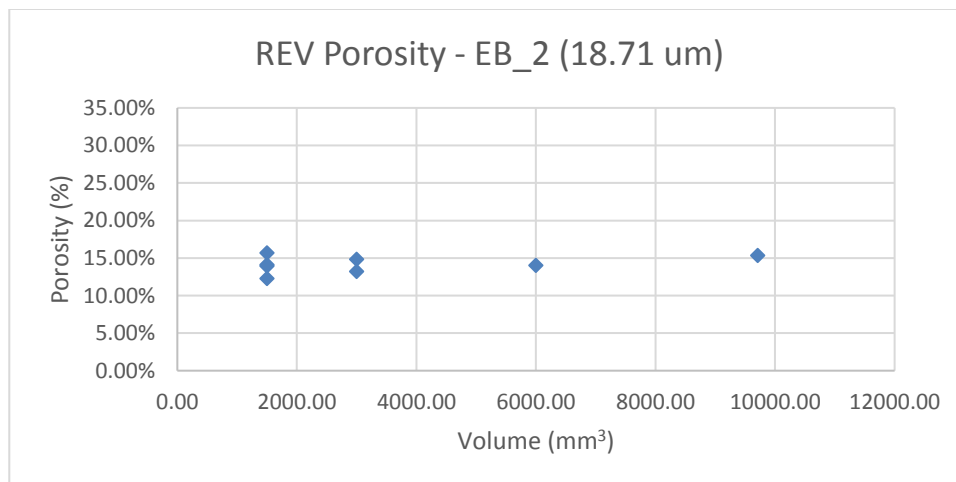


Figure 17: REV analysis for porosity of sample EB_2.

REV analysis - Permeability

Pore network modeling and fluid flow simulations for the obtaining permeability were performed using PoreFlow to the same 1 sample and 15 subsamples volumes from the coquina 1_34A. The results are plotted in the Figure 18 against the sample volume. The results indicate an increase in permeability variation as the sample volume decrease. The results for the eight 1700 mm³ squares vary up to one order of magnitude above and below. Considering the variability of permeability as a log distribution, subsamples volumes above 6900 mm³ were found to be at the same order of magnitude from the lab experiments. However, only volumes above 13700 mm³ were able to represent the laboratory measured value for this sample, considering a maximum variation of 196 mD.

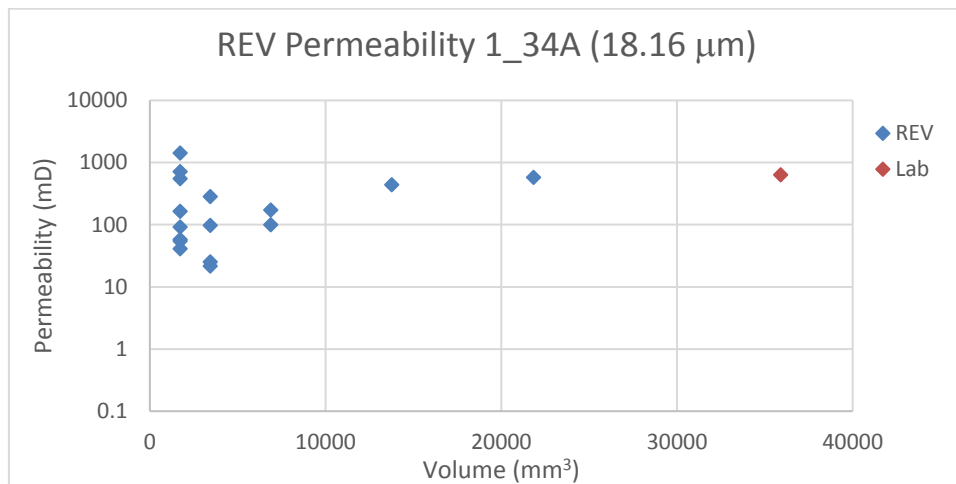


Figure 18: REV analysis for permeability of sample 1_34A.

The pore network models and fluid flow simulations were performed for the 1 sample and 6 subsamples of the slab EB_1, the results for permeability are plotted against sample volume in the Figure 19. The results indicate an increase in permeability variation as the sample volume decrease, however, even for the largest volume the result is one order of magnitude higher than the value measured in laboratory. Therefore, the slab sample of the Edwards Brown carbonate, EB_1, cannot be considered as REV for permeability.

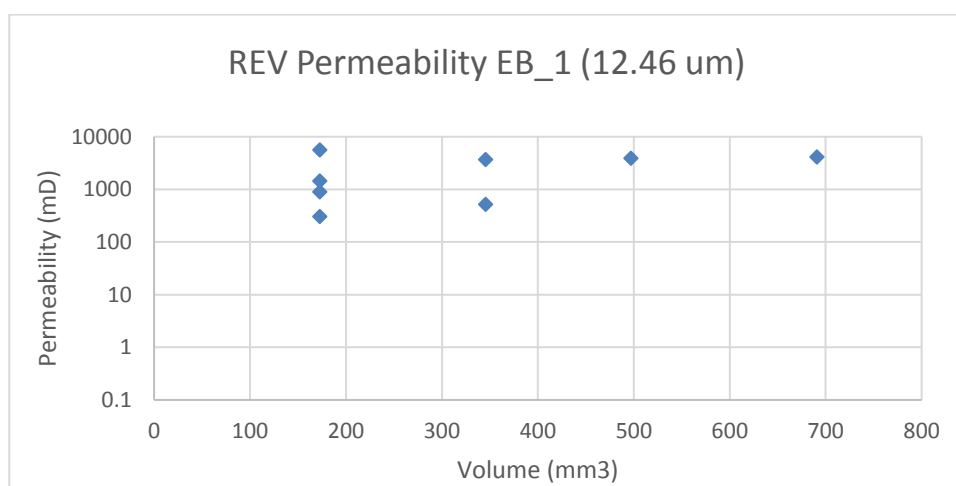


Figure 19: REV analysis for permeability of sample EB_1.

Pore network modeling and fluid flow simulations for the obtaining permeability were performed for 1 sample and 15 subsamples volumes from the plug EB_2. The results are plotted in the Figure 20 against the sample volume. The results indicate an increase in permeability variation as the sample volume decrease and also present a decrease of permeability. The results for the volumes below 3000 mm³ vary up from the same order of magnitude of the lab measurement up to one order below. The only samples that presented results at the same order of magnitude from the lab measurement comprehends volumes above 6000 mm³. Therefore, only measurements above this volume can be considered to present higher confidence, considering a maximum variation of 93 mD from the lab measurement. If results were compared to the coquina, samples of around 6900 mm³ presented a variation between 466 and 538 mD, thus the scale of heterogeneity of the coquina may be larger than the Edwards Brown samples. Although this sample presented a high variability for porosity, porosity and permeability's REV were found at the sample subsample volume.

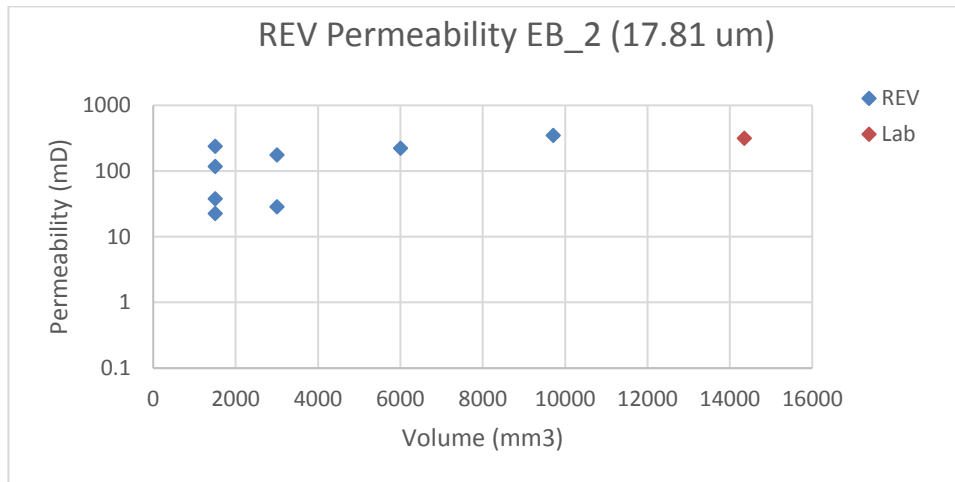


Figure 20: REV analysis for permeability of sample EB_2.

4 Conclusions

The micro-CT images added by the information brought from NMR T_2 experiments enabled the study of the pore networks in terms of porosity, permeability and their respective representative elementary volume (REV) for three carbonate samples. RCA experiments were also performed and used as correlation for the digital models' estimations, as well as understanding the higher presence of microporosity in the samples of Edwards Brown.

The plug samples were analyzed by images with approximately the same resolution, while the EB sample also was analyzed by a slab size sample with images of higher resolution. The micro-CT images from these three samples were processed and segmented using three different methods: manual, Otsu's algorithm and NMR guided. The latter, was considered to have a good reliability and was selected to the final threshold of segmentation of the images. From that, the micro-CT images were analyzed to estimate porosity and permeability, which was determined after the modeling and simulation of PNM using PoreFlow.

The digital models of the rock samples were later partitioned in several subsamples and studied for REV analysis. Porosity REV was found for the coquina sample 1_34A for volumes above 3400 mm³, with a 94% confidence, while the samples of EB_1 presented 99% of confidence, in terms of porosity variation, in volumes above 350 mm³. The sample EB_2 presented a high heterogeneity, mainly due to the high presence of shells in its volumes, therefore only volumes above 6000 mm³ presented a confidence that porosity would not vary more than 10%.

REV analysis was also performed considering the rock property of permeability. Opposite to porosity, this property presents a log scale variation and thus, it was expected to require large volumes to be considered as REV. This was observed for sample EB_1, where even when the entire sample was considered for permeability estimation, it presented results one order of magnitude higher than the lab measurements. Therefore, this sample could not be considered as REV. The plug samples, 1_34A and EB_2 presented a higher confidence. The subsamples with volume superior to 6900 mm³ from 1_34A did not presented a variation of one order of magnitude and could be considered as REV. The same was observed for the subsamples above 6000 mm³ of EB_2.

Acknowledgements

The authors would like to acknowledge the support from CAPES and the reaseach teams from LRAP/COPPE/UFRJ, LIN/UFRJ and UFFlar/UFF. Additionally, we would like to thank the collaboration of Dr. Amir Raouf, from Utrecht University, for the technical discussions and for making the software PoreFlow available.

References

- [1] Schlumberger. Carbonate Reservoirs. Available in https://www.slb.com/services/technical_challenges/carbonates.aspx. Visited in August 6, 2018
- [2] Hurley, N. F., Zhao, W, Zhang, T. Multiscale Workflow for Reservoir Simulation. SPWLA 53rd Annual Logging Symposium, June 16-20, 2012.
- [3] Vik, B, Bastesen, E., Skauge, A. Evaluation of Representative Elementary Volume for A Vuggy Carbonate Rock—Part: Porosity, Permeability, And Dispersivity. *Journal of Petroleum Science and Engineering*, v. 112, pp. 36–47, 2013.
- [4] Corbett, P.W.M., Anggraeni, S., Bowden, D. The Use of The Probe Permeameter In Carbonates-Addressing the Problems of Permeability Support and Stationarity. *Log Anal.*, v. 40 (5), pp.316–326, 1999.
- [5] Corbett, P.W. Integration of Static and Dynamic Models. *Petroleum Geoengineering. SEG/EAGE Distinguished Instructor Series*, v. 12, pp. 100–190, 2009.
- [6] Bear, J. *Dynamics of Fluids in Porous Media*. Dover, New York, 1988.
- [7] Bultreys, T., Boever, W., Cnudde, V. Imaging and image-based fluid transport modeling at the pore scale in geological materials: A practical introduction to the current state-of-the-art. *Earth-Science Reviews*, v. 155, pp. 93–128, 2016.
- [8] Blunt, M.J. Flow in Porous Media — Pore-Network Models and Multiphase Flow. *Current Opinion in Colloid & Interface Science*, v. 6, pp. 197–207, 2001.
- [9] Raouf, A., Nick, H.M., Hassanizadeh, S.M., Spiers, C.J. PoreFlow: a complex pore-network model for simulation of reactive transport in variably saturated porous media. *Comp. Geosciences*, v. 61, pp. 160–174. <http://dx.doi.org/10.1016/j.cageo.2013.08.005>., 2013
- [10] Raouf, A., Hassanizadeh, S. M. A new method for generating pore-network models of porous media. *Transport in Porous Media*, v 81(3), pp. 391–407, 2009.
- [11] Vries, E. T., Raouf, A., van Genuchten, M. T. Multiscale modelling of dual-porosity porous media; a computational pore-scale study for flow and solute transport. *Advances in Water Resources*, v. 105, pp. 81-95, 2017.
- [12] Kenyon, W. E. Petrophysical principles of applications of NMR logging. *The Log Analyst*, 38(02), 1997.
- [13] COATES, G. R., XIAO, L., & PRAMMER, M. G. NMR logging: principles and applications, Vol. 344, Haliburton Energy Services, Houston, 1999.
- [14] Souza, A. Estudos de Propriedades Petrofísicas de Rochas Sedimentares por Ressonância Magnética Nuclear. Phd Thesis, USP, São Paulo, Brazil, 2012.
- [15] Souza, A., Carneiro, G., Boyd, A., Hurlimann, M., Trevizan, W., Coutinho, B., Machado, V., Bagueira, R. Improving Lab Nmr Petrophysical estimations By Incorporating the Surface Relaxivity Parameter. International Symposium of the Society of Core Analysts held in Snowmass, Colorado, USA, 21-26 August 2016
- [16] Hoerlle, F., Silva, E., Rios, Silva, W., G., Pontedeiro, E.M., Lima, M. C. O., Corbett, P., Alves. J., Couto, P. Nuclear Magnetic Resonance to Characterize the Pore System Of Coquinas from Morro do Chaves Formation, Sergipe-Alagoas Basin, Brazil. *Revista Brasileira de Geofísica*, v. 36(3), pp. 1-8, 2018.
- [17] Hoerlle, F., Silva, W., Rios, E., Silveira, T., Couto, P. Alves. J. Lima, M., Corbett, P. Evaluation of Segmentation Procedures Using X-Ray Computed Microtomography Images Of Coquinas From Morro Do Chaves Formation – Ne Brazil. *Cilamce 2017*, Florianopolis, Brazil, 2017.
- [18] Godoy, W., Pontedeiro, E. M., Hoerlle, F., Raouf, A., Genunchten, M. T, Santiago, J. Couto, P. Computational and experimental pore-scale studies of a carbonate rock sample. *J. Hydrol. Hydromech.*, 67, 2019, 4.
- [19] Luna J, Perosi F.A, dos Santos Ribeiro M.G, Souza A, Boyda A, de Almeida L.F.B. & Corbett P.W.M. 2016. Petrophysical Rock Typing of Coquinas from the Morro do Chaves Formation, Sergipe-Alagoas, 2016. Basin (Northeast Brazil). *Revista Brasileira de Geofísica*, 34(4): 509–521.
- [20] Thermo Fisher Scientific. Avizo 9.5.0 Reference Manual, 2018.

[21] Kurotoria, T., Zahaskyc, C., Bensonc, S. M., Pini, R. Three-Dimensional Imaging of Solute Transport in Reservoir Rocks by Positron Emission Tomography. 14th International Conference on Greenhouse Gas Control Technologies, GHGT-14, Australia, 2018.